Aggregation and Disaggregation Kinetics of Human Blood Platelets: Part III. The Disaggregation under Shear Stress of Platelet Aggregates

Pin Y. Huang* and J. David Hellums
Cox Laboratory for Biomedical Engineering, Rice University, Houston, Texas 77251-1892 USA

ABSTRACT In the preceding two papers (1, 2), a population balance equation (PBE) mathematical model was developed, validated, and applied to the analysis of platelet aggregation kinetics under the influence of hydrodynamic shear stress. The present work involves the application of the model to the analysis of platelet reactions under shear stress in circumstances where disaggregation processes are of dominant importance: the disaggregation of aggregates formed in response to added agonists. Aggregation-disaggregation experiments were performed in the constant shear field of a rotational viscometer, and the evolution of the particle size distribution was determined by use of an electronic particle counter. The PBE model was used to simulate the experimental results. Exploratory calculations made it possible to reduce a rather complete, complex model to a more tractable form which retains the capability of simulating the experimental observations. For the experimental conditions studied, disaggregation by a splitting mechanism was found to be of dominant importance. The surface erosion mechanism can be neglected without significant impact on results. Physical reasoning confirmed by exploratory calculations showed that a discontinuous form of the breakage rate expression which incorporates a minimum friable particle size, gives significantly better results than a continuous expression. A simple step function void fraction parameter was found to be at least as successful as a more complicated, continuous function.

The resulting simplified model has the potential of increasing our understanding of kinetics and mechanisms of platelet reactions, and of characterizing the state of platelet activity. Hence, it may be useful in efforts to understand thrombotic and hemostatic processes.

INTRODUCTION

This paper is the last of a set of three on studies of platelet aggregation and disaggregation kinetics under the influence of hydrodynamic shear stress. In Part I (1), a mathematical model for analyzing platelet aggregation kinetics was developed and validated. In Part II (2), platelet aggregation and related reactions were studied in the uniform, known shear stress field of a rotational viscometer. Platelet kinetics results were interpreted by means of the population balance equation (PBE). Under the shear conditions of Part II, good agreement was obtained between experimentally observed and calculated values of the particle size distributions. This good agreement was obtained with either the reversible or the irreversible model. This finding suggests that aggregate breakage processes were of only secondary importance under the conditions studied. Therefore, studies to be described in this paper were undertaken under conditions for which it was known that aggregate breakage processes are important: the disaggregation in a shear field of platelet aggregates previously formed in response to low dosage of ADP.

The breakage of flocs or aggregates is a complicated process, and information on the breakage distribution functions was scarce until recently. Most literature covering the breakage of particles comes from the study of industrial processes such as ore comminution, powder grinding and crushing, and water treatment processes (3, 4). In some of these studies, breakage relationships are drawn from analogies between droplet coalescence and breakage. Due to the fundamental differences between drops, flocs, and platelet aggregates, caution must be exercised in the development of kernels for breakage. The development must be guided by experimental observations.

The earliest efforts to characterize floc breakup from a microscopic viewpoint were those of Argaman and Kaufman (5) and Parker and Kaufman (6): two different modes of floc breakup (surface erosion and splitting mechanisms) were described. Kao and Mason (7) observed dispersion of assemblages of noncohering plastic spheres suspended in silicone oil subjected to both uniform laminar shear and extensional flow fields. They found that the measured radius of the assemblage continuously decreased with time as constituent spheres were pulled off (erosion) along the principal axes of extension. Quigley (8) performed experiments similar to those of Kao and Mason and reported that aggregates simultaneously exhibited both erosion and splitting into smaller aggregates. The importance of breakage in process applications was clearly demonstrated by experiments such as those of Andrea-Villegas and Letterman (4). They observed the net rate of particle aggregation increased and then decreased as the rate of agitation increased in batch experiments.

Glasgow and Luecke (9) studied mechanisms of degradation for clay-polymer flocs in turbulent systems, and concluded that the breakup resulted primarily from the hydrodynamic shear stress. They suggested that flocs subjected to

Received for publication 25 June 1992 and in final form 11 February 1993.
Address reprint requests to J. H. Hellums.
* P. Y. Huang is now with Exxon Production Research, Houston, TX 77252-2189.

0006-3495/93/07/354/08 $2.00

high energy dissipation rates tend to become more regular in conformation, proposing that appendage fracture occurs rather than the massive splitting proposed by Thomas (10).

Following the approach taken by Valentas et al. (11) for droplet breakage, Pandya and Spielman (12, 13) applied the population balance equation to the study of Kaolin-hydrous ferric-oxide flocs (1–100 μm in diameter) undergoing breakage in an agitated batch system. The experimentally determined size distributions were fitted to those computed from the population balance equation, using constrained nonlinear least squares. The breakage frequency $g(v)$ was found to vary as the 0.71 power of the shear rate and the 0.33 power of the parent floc volume.

Akers et al. (14) applied a similar equation to study the floc size distribution (FSD) of aggregated latex particles subjected to a step change in turbulent energy. During exposure to turbulence, there was a broadening of the FSD and a new equilibrium was approached. For short periods of exposure to turbulent flow, the evolving shape of the FSD was determined primarily by the splitting mechanism. The FSD reached an equilibrium that did not seem to be the point of balance between aggregation and disruptive process, but was limited to a distribution at which the splitting failed to produce further fragments. Thus, the breakage rate was not determined solely by size.

Pandya and Spielman (12, 13) studied the kinetics of breakage of clay-$Fe(OH)_3$ flocs by erosion. By assuming that the erosion process is volume-conserving, and that the particle size distribution of the eroded particles is given by a log normal distribution, they derived expressions for the instantaneous rate of change of the volume of a parent particle and for the total rate of formation of erosion fines of all sizes, per eroding particle. The gradual emergence of a peak in the small particle region of a size distribution supported the occurrence of erosion mechanism. In their studies, the erosion rate was found to be independent of shear rate. The erosion rate reported for kaolin-ferric hydroxide system is about 10^{-6} times that reported for noncohesive spheres. This finding demonstrates that the presence of interparticle forces drastically reduced the erosion rate.

Nichols and Bosmann (15) reported disaggregation of large human platelet aggregates by the dispersal of singlets and small aggregates from the periphery of aggregates. This mechanism, however, would not account for the large volume shifts of the large aggregates that were observed. Nguyen and O'Rear (16) analyzed blood platelet aggregation and disaggregation kinetics using population balance mathematics. The approach was somewhat similar to that given here, but it was limited to aggregation processes in Brownian motion, and used a discrete (rather than continuous) form of the population balance.

EXPERIMENTAL METHODOLOGY

Many aspects of the experimental methodology are similar to those of Part II (2). The experimental procedure consists of six steps: 1) preparation of platelet suspension, 2) aggregation of the suspension by addition of low dosages of adenosine diphosphate (ADP), 3) sampling of the aggregated specimen to yield the "initial" particle size distribution for the disaggregation process, 4) disaggregation of the specimen in the shear field of the rotational viscometer, 5) sampling of the specimen to yield the disaggregated particle size distributions, and 6) mathematical analysis of the results to determine population balance parameters for the disaggregation processes.

The cone and plate viscometer used in this work is represented schematically in Fig. 1. The key feature of the apparatus is the optical system which permits monitoring of light transmission and light scattering. This feature makes it possible to establish values of the shear rate, ADP dosage, and the post-ADP time such that significant, but reversible, aggregation was obtained in a reproducible way. Platelet aggregation experiments were carried out at 37°C with low doses of ADP. After preincubation of PRP samples in a water bath for 5 min, 1.1 ml of sample was loaded onto the modified glass platen with a 1° cone (Fig. 1). Details of the design and experimental procedures are given by Huang (17). The modified glass platen consists of a cylindrical glass tubing section sitting on a quartz plate. The inner diameter of the glass tubing was polished to a specific dimension (Optical Instrument Laboratory, Houston, TX) so that the shear rate experienced by the platelets in the suspension is the same in the cone-plate and annulus regions. Control samples and aggregated samples were taken from the injection port at 60-s intervals using multiplex microcapilliary pipettes (PGC Scientifics, Gaithersburg, Maryland). The desired dose of ADP was determined to be about 0.25 μM in final concentration by a trial and error technique. The desired concentration of ADP was defined to be that which gives extensive aggregation in 60 s and extensive reversal of the aggregation at 120 s (see Fig. 2).

The inset in Fig. 3 gives the light transmission signal schematically for a typical experiment. At time 0, point A in the figure, a low dosage of ADP was added to the platelet suspension in the viscometer. During the time interval A to B, typically about 60 s, the suspension aggregated as indicated by the increase in transmitted light. Subsequently, the suspension began disaggregation as indicated by the decrease in transmitted light after point B. Point B represents the initial condition (zero time) for the disaggregation process studied in this work. A sample of the suspension taken at this time was analyzed for particle size distribution and designated as the initial distribution. Subsequently, samples were taken (at point C for example) and designated as the final condition after various stages of the disaggregation process. The steps in the procedure are given below as follows.

1. Platelet suspensions were subjected to a uniform shear rate of 450 s^{-1} (about 7 dynes/cm^2) in the cone-plate viscometer using the glass platen.

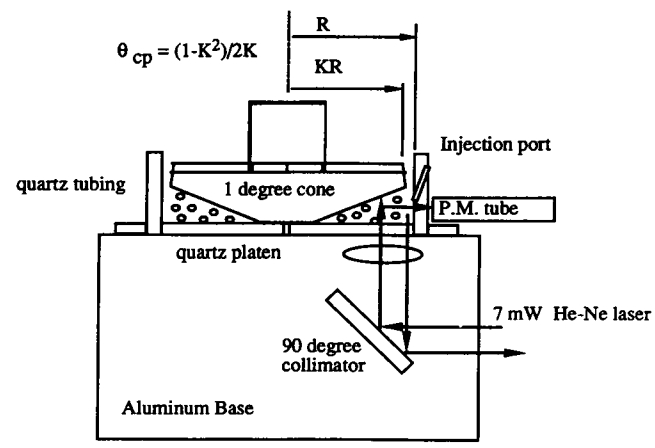

FIGURE 1 Schematic of cone-plate viscometer with the modified bottom platen for measurement of light transmission and light scattering. θcp is the cone angle in radians, and K is the ratio of the radii of the inner and outer cylinders of the annulus. For the 1° cone used in this work, KR = 3.5000 cm, and R = 3.5616. Sample volume is 1.1 ml.

2. At time 0, ADP was added to the platelet suspension.

3. At 60 s, 60 μl of aggregated sample was drawn into 80 ml of glutaraldehyde-isoton solution (0.25% w/v). At this time, the maximum extent of aggregation existed as judged by monitoring of optical density.

4. At 120 s, another 60 μl of aggregated sample was drawn into 80 ml of glutaraldehyde-isoton solution (0.25% w/v). At this time, substantial disaggregation had occurred as judged by monitoring of optical density.

5. The particle size distributions were determined with the Coulter Multisizer.

6. The particle size distribution obtained at 60 s was used as initial condition in the simulation program to generate the particle size distribution at 120 s. Parameter search methods as described in Part I (1) were used to get the "best" agreement between observed and calculated size distributions.

RESULTS

Experimental results

Fig. 2 gives a typical volume density distribution versus time for a disaggregation experiment. At time 0 (*solid line*), the initial platelet size distribution is apparently normal. At 60 s (*dashed line*), the initially narrow particle size distribution spreads to the right to form a bimodal distribution. The new peak represents large aggregates which grew by inclusion of small aggregates and singlets. Considerable disaggregation has occurred at 120 s (*line* with *dashes and dots*). Large aggregates are diminished in number and size, and the mode of the aggregate peak is shifted leftward. Particles in the singlet region are markedly increased.

Sensitivity studies and simplified model

Sensitivity studies were carried out in a manner analogous to those described previously (1). The results showed that, for the disaggregation experiments, the calculated values of the collision efficiency are several orders of magnitude lower than calculated for shear-induced platelet aggregation. This finding shows that the aggregation terms are not important in the analysis of this particular disaggregation process. Results from other parameter sensitivity analyses (to be discussed later) also showed that the erosion mechanism of particle breakup is not important in studying these processes. These findings show that attention may be confined to breakage by the splitting mechanism. Thus, for the modeling of the disaggregation experiments, it was possible to use the simplified equation given below:

$$\frac{\partial n(v,t)}{\partial t} = \int_v^\infty n(w,t)\gamma(w)g(w)p_s(w,v)\mathrm{d}w - n(v,t)g(v) \quad (1)$$

where $0 \le t < \infty$, $v_s \le v < \infty$.

Basic comparison of calculated and experimental results

Before discussing the results, we will review the principal parameters associated with the problem. ϕ_a is the maximum void fraction in the void fraction expression (defined in Eqs. 2 and 3 below). It serves to inflate the collision diameter of the platelet aggregates to account for their irregular (nonspherical) shape. k_1 and m are breakage rate coefficient and exponent, respectively (defined in Eq. 4 below). γ is the average number of daughter fragments resulting from splitting of an aggregate. $\tilde{k}$ is the erosion rate coefficient (defined in Eq. D of the accompanying article (Part I) (1)).

Calculations to assess the importance of the erosion mechanism were carried out by use of an augmented version of Eq. 1. Equation 1 is based on only splitting breakage mechanism. It was augmented by addition of the erosion mechanism terms: Equations *A* and *C* from the Appendix of the first paper (Part I) of this set (1). Fig. 3 gives a comparison of experimental and calculated volume density distributions for the disaggregation process. The aggregated sample was obtained by subjecting the PRP (320,000 platelets/μl) to a final ADP concentration of 0.25 μM. The initial condition (open squares) corresponds to maximum aggregation as indicated by *B* in the inserted light transmission curve. Similarly, the disaggregated sample (open circles) corresponds to *C* in the transmission curve. The disaggregated sample is obtained 2 min after ADP addition. The computed curve that accounts for breakage by splitting and erosion is given by open triangles. The erosion rate coefficient is estimated to be about 6×10^{-11} which is consistent with our assumption that we may neglect the erosion processes. Hence, the equations for the erosion mechanism were relegated to the Appendix of the

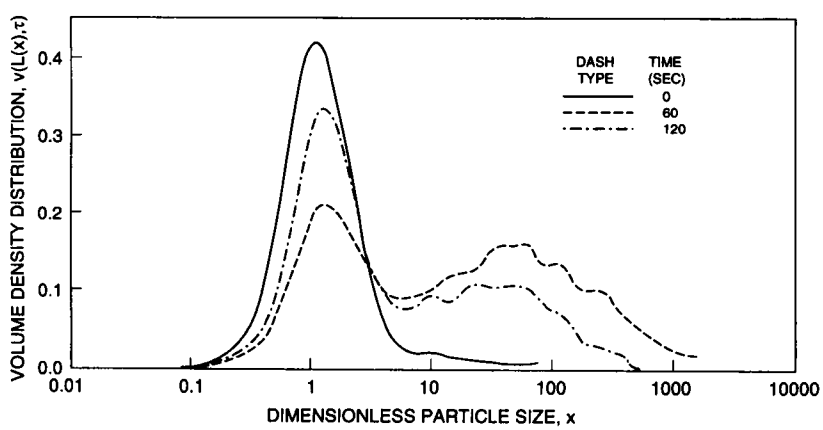

FIGURE 2 Progression of particle volume density distribution for reversible ADP-induced aggregation of PRP at 37°C. (final concentration of 0.25 μM ADP). The aggregated condition at 60 s is treated as the initial condition for study of disaggregation kinetics for the subsequent period.

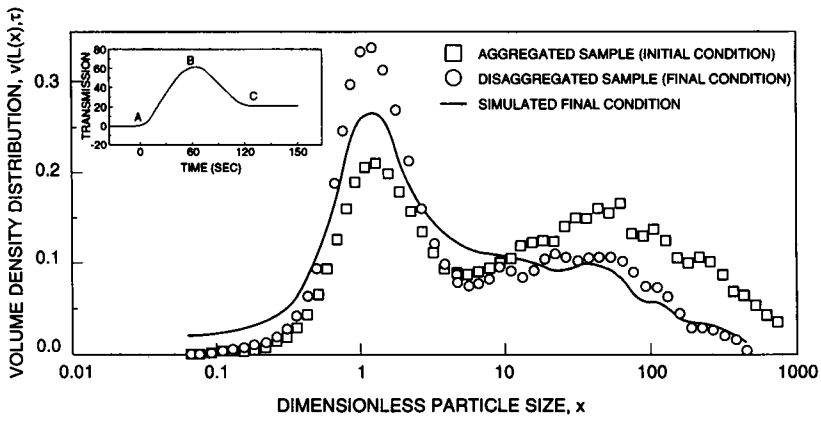

FIGURE 3 Comparison of observed and calculated volume density histograms for the disaggregation phase of reversible aggregation induced by ADP (final concentration of 0.25 μM) at 37°C: (□) Experimental histogram for the aggregated sample (initial condition); (○) histogram for the disaggregated sample (final condition); (–) simulated final condition with $\phi_a = 0.95$, $k_1 = 4.3 \times 10^{-3}$, $\tilde{k} = 6.2 \times 10^{-11}$, $m = 0.38$, and $\gamma = 10.8$. All histograms other than the initial histogram have same dimensionless volume and time. The inset schematically gives the transmission of light through a specimen as the processes occur. *A* denotes the unaggregated platelet suspension. *B* denotes the aggregated sample 1 min after addition of ADP (the initial condition). *C* denotes the disaggregated sample (the final condition).

first paper (1) and not included in Eq. 1. Subsequent results to be discussed here did not include the erosion mechanism.

Figs. 3, 4, and 5 represent typical comparisons between the model simulations and experimental observations using the continuous form of the breakage rate expression, $g(x)$ given in Eq. 4 below. In these figures, the reversible model projects the breakage of large aggregates to form an assortment of daughter fragments including singlets ($x = 1$), small aggregates ($2 < x < 10$), and intermediate aggregates ($10 < x < 100$). The model correctly predicts the trends including the shifting of the aggregate peaks. However, the model grossly underestimates the number of singlets and overestimates the numbers of both fragments ($x < 1$) and small aggregates ($2 < x < 10$).

Forms of the void fraction expression

The overestimation of the presence of subplatelet-sized particles ($x < 1$) from the model can partially be explained from the studies on the parameter sensitivity of ϕ_a, k_1, γ, and m. Yet, it cannot explain why the model has grossly overestimated the presence of small aggregates. Results from sensitivity analysis suggested that both the breakage rate constant and void fraction play important roles in the model. Therefore, study is focused on these parameters and on the mathematical expressions for these parameters. As mentioned in the parameter sensitivity analysis of Part I (1), a 10% increase in the values of ϕ_a, k_1, and m resulted in the formation of fragments or debris with sizes less than $x = 0.8$, and shifting of the large aggregate peak to the left. Changing the value of x where the discontinuity occurs in the expression for $\phi(x)$, see Eq. 2 below, from 2 to 4.5 resulted in prediction of fewer fragments smaller than $x = 0.8$. But this reduction in the numbers of fragments was balanced by more of the small, intermediate, and larger aggregates which resulted in poor curve fitting at other particle size ranges. These findings suggest that the step function form may not be adequate for describing ϕ. Replacing the step functional form for ϕ with a linear, continuous function was studied. Figs. 3 and 6 give comparisons between calculated and experimentally observed volume density distributions using step and linear expressions for $\phi(x)$. In these studies, values for pa-

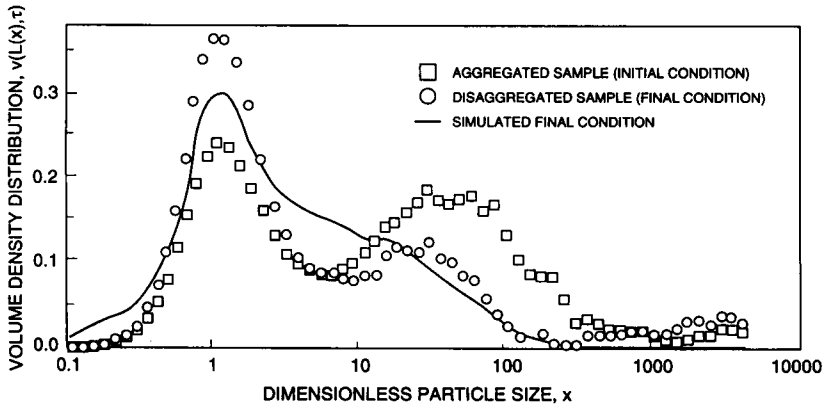

FIGURE 4 Comparison of observed and calculated volume density histograms for the disaggregation phase of reversible aggregation induced by ADP (final concentration of 0.25 μM) at 37°C: (□) Experimental histogram for the aggregated sample (initial condition); (○) histogram for the disaggregated sample (final condition); (–) simulated final condition with $\phi_a = 0.78$, $k_1 = 3.4 \times 10^{-3}$, $\tilde{k} = 1.4 \times 10^{-11}$, $m = 0.53$, and $\gamma = 14.6$. All histograms other than the initial histogram have same dimensionless volume and time.

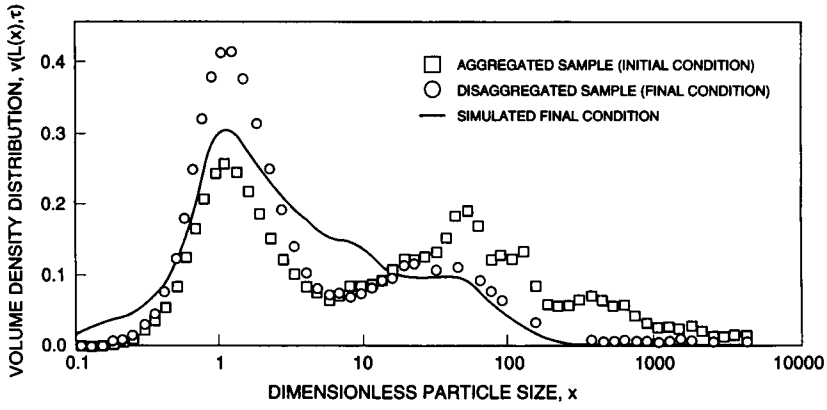

FIGURE 5 Comparison of observed and calculated volume density histograms for the disaggregation phase of reversible aggregation induced by ADP (final concentration of 0.25 μM) at 37°C: (□) Experimental histogram for the aggregated sample (initial condition); (○) histogram for the disaggregated sample (final condition); (–) simulated final condition with ϕ_a = 0.76, $k_1 = 1.4 \times 10^{-3}$, $\tilde{k} = 1.4 \times 10^{-10}$, m = 0.62, and γ = 12.9. All histograms other than the initial histogram have same dimensionless volume and time.

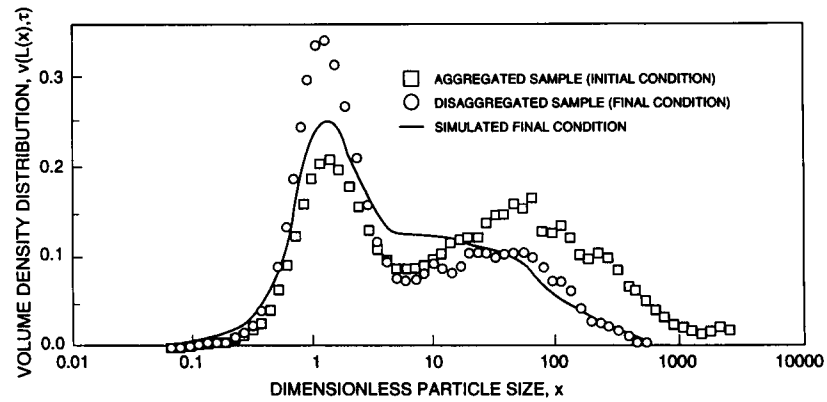

FIGURE 6 Progression of particle size distribution calculated by the reversible model using a linear form of $\phi(x)$: $\phi(x) = 0$ for $x \leq 1.5$, $\phi(x) = \phi_a(x - 1.5)/3$, for $1.5 \leq x \leq 4.5$, and $\phi(x) = \phi_a, x > 4.5$ (□) Experimental histogram for the aggregated sample (initial condition); (○) histogram for the disaggregated sample (final condition); (–) simulated final condition with ϕ_a = 0.95, $k_1 = 4.3 \times 10^{-3}$, $\tilde{k} = 6.2 \times 10^{-11}$, m = 0.38, and γ = 10.8. All histograms other than the initial histogram have same dimensionless volume and time. The results of this figure may be compared to those of Fig. 3 which is on the same basis except for the use of the simpler,discontinuous form of $\phi(x)$ given by Eq. 2.

rameters k_1, m, γ, and $\tilde{k}$ were the same. For the results of Fig. 6, $\phi(x)$ was given by Eq. 3, whereas the results of Fig. 3 and elsewhere in this work used the form of Eq. 2.

$$\phi(x) = \begin{cases} 0, & x < 2 \\ \phi_a, & x \geq 2 \end{cases} \tag{2}$$

$$\phi(x) = \begin{cases} 0, & x < 1.5 \\ \phi_a(x - 1.5)/3, & 1.5 \leq x \leq 4.5 \\ \phi_a, & x > 4.5 \end{cases} \tag{3}$$

By comparing with Figs. 3 and 6, it can be seen that the linear form of $\phi(x)$ gave a better fit in the small particle size range ($x < 1$). The linear form also gave good agreement in the large particle size range ($x > 20$). Nevertheless, the problem of overestimating the small aggregates ($2 < x < 10$) remained, and the overall agreement with experiment was not improved by use of the continuous form, Eq. 3.

Forms of the breakage rate expressions

The mathematical form of the breakage rate, $g(x)$, defined by Eq. 4 (Eq. 22 in Huang and Hellums (1)) was examined. Fig. 7 gives calculated particle size distributions as a function of dimensionless time, τ, using the continuous breakage rate, Eq. 4. The model predicts the breakage of large aggregates to give assorted daughter fragments including singlets and small aggregates, and shifting of the large aggregate peak to the left. The changes result in the accumulation of aggregates in the particle size range of 2 to 10. The model correctly predicts the breakage of large aggregates to form small and intermediate aggregates. Unfortunately, the model also predicts the breakage of singlets to form debris smaller than single platelets ($x < 1$) and fails to predict sufficient breakage of small aggregates in size range of $2 < x < 20$. Comparison with experimental distributions suggests that an improved form of the breakage rate should predict more breakup of small aggregates ($4 < x < 10$), and much less breakup of singlets and doublets. These needs and physical reasoning suggest a discontinuous form of the breakage kernel.

Replacing the continuous form of $g(x)$ defined in Eq. 4

$$g(x) = k_1 \left(\frac{x}{1 - \phi} \right)^m \tag{4}$$

with a discontinuous formulation defined by Eq. 5 (Eq. 24 in Huang and Hellums (1))

$$g(x) = \begin{cases} k_1 \left(\dfrac{x}{1 - \phi} \right)^m, & \text{for } x > x_{ss} \\ 0, & \text{for } x \leq x_{ss} \end{cases} \tag{5}$$

improved the fit, especially between $x = 2$ and $x = 20$. In the discontinuous form of $g(x)$, the breakage rate is zero for particle sizes less than a dimensionless maximum stable size, $x_{ss} = 1.5$. Overall, the improvement reduces the objective

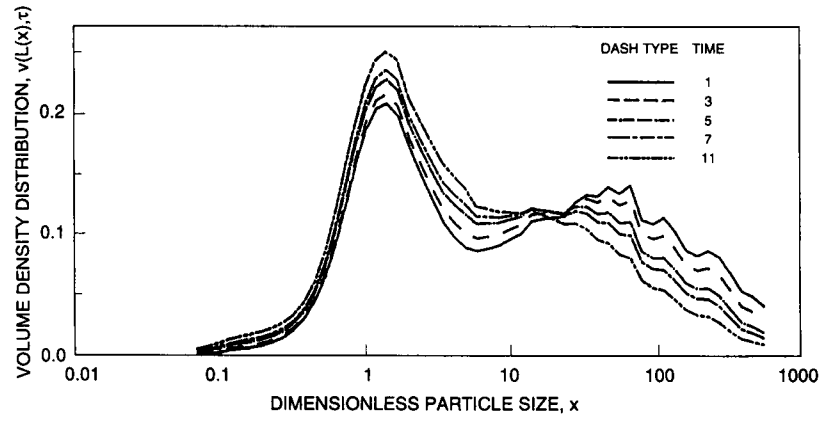

FIGURE 7 Progression of particle size distribution calculated by the reversible model using the continuous form of breakage rate, Eq. 4. Values of the parameters used in the calculation are: $\phi_a = 0.64$, $k_1 = 4.5 \times 10{-}3$, $\tilde{k} = 9.6 \times 10^{-3}$, $m = 0.4$, and $\gamma = 14.5$.

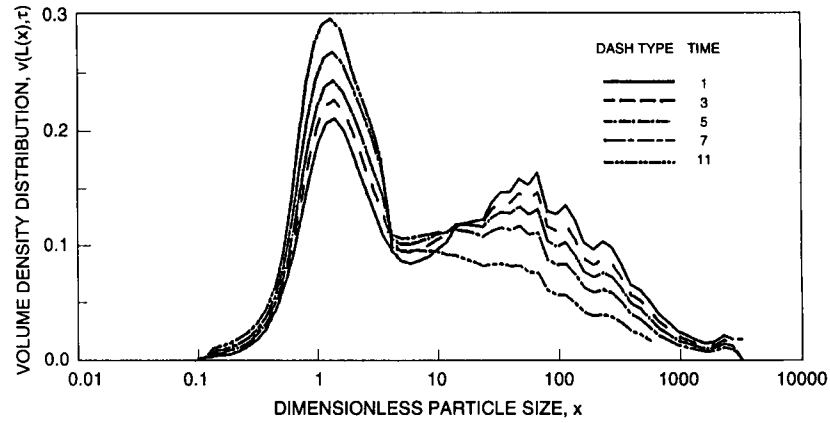

FIGURE 8 Progression of particle size distribution calculated by the reversible model using the discontinuous form of breakage rate (Eq. 5 with $x_{ss} = 1.5$). The results of this figure may be compared to those of Fig. 7 which are on the same basis except for the form of breakage rate expression.

function by 50 to 60%. Fig. 8 (discontinuous $g(x)$) gives a particle size distribution versus time for the same case as Fig. 7 (continuous $g(x)$). Using the discontinuous breakage rate, the model predicts the sequential breakdown of large aggregates to intermediate and small aggregates. Furthermore, the model predicts the breakage of small aggregates ($x > 1.5$) to form singlets and relatively few smaller particles.

Fig. 9 gives comparisons between calculated and experimentally observed volume density distributions using the discontinuous breakage rate expression. Error bars which represent the standard error of the mean from a minimum of seven repeated experiments are shown in the figure. Replacing $g(x)$ with a discontinuous formulation resulted in much better agreement with the experimental findings by more nearly correct treatment of the disappearance of small aggregates.

The mean values of the population parameters are summarized in Table 1, as obtained from six different donors. Under the conditions studied, the breakage rate constant $k_1(x)$ is 0.004. This translates to about 11 breakages/100 par-

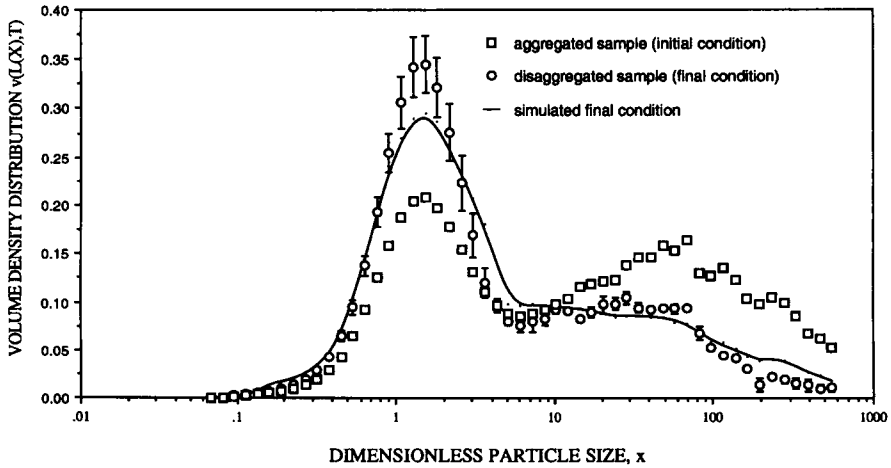

FIGURE 9 Comparison of observed and calculated volume density histograms for the disaggregation phase of reversible aggregation induced by ADP (final concentration of 0.25 μM) at 37°C: (□) Experimental histogram for the aggregated sample (initial condition); (○) histogram for the disaggregated sample (final condition); (–) simulated final condition with $\phi_a = 0.95$, $k_1 = 4.0 \times 10^{-3}$, $\tilde{k} = 6.6 \times 10^{-6}$, $m = 0.02$, and $\gamma = 6.7$. All histograms other than the initial histogram have same dimensionless volume and time.

TABLE 1 Estimates of population balance parameters for the disaggregation phase of ADP-induced, reversible platelet aggregation

Parameter	Mean	Mean ± SE
k_1	4.3×10^{-3}	1×10^{-3}
$\tilde{k}$	3.8×10^{-4}	2.66×10^{-4}
m	0.105	0.045
γ	11.7	2.9
ϕ	0.915	0.02

Estimates for each parameter represents the mean from six different donors. For each donor, three to eight replicate experiments were carried out.

ticles of size $x = 1000/s$. Each such breakage produces about 12 daughter fragments and with a mean volume of $x = 85$ (volume of 85 single platelets).

DISCUSSION

This work seems to be the first to apply population balance methods to the study of the disaggregation of platelet aggregates in a laminar shear field. Disaggregation is inherently complicated, and a comprehensive model which incorporates disaggregation as well as aggregation must involve a large number of parameters. In this work we have taken a rather complete, complex model, and, by use of exploratory calculations, modified it and reduced it to a more tractable form. The reduced PBE retains the capability to simulate the experimental observations of this work: disaggregation under shear stress of platelet aggregates formed in response to low dosage ADP.

For the experimental conditions studied, it was determined that the particle size distributions and population balance parameters were virtually independent of the collision efficiency parameter. This finding was corroborated in the parameter sensitivity studies. The finding yields the conclusion that disaggregation processes (not aggregation) dominate in the experimental conditions studied, and results in an important simplification of the PBE. Another major simplification of the PBE followed from sensitivity studies on the mechanism of disaggregation: the particle splitting mechanism was found to be of dominant importance. Thus, the surface erosion mechanism with its considerable complication can be neglected without significant impact on results.

A simple step function form of the void fraction parameter (Eq. 2) was found to be at least as successful as a more complicated, continuous function (Eq. 3).

Exploratory calculation revealed that a discontinuous form of the breakage rate expression (Eq. 5), which incorporates a minimum friable particle size, gives significantly better results than a continuous expression, Eq. 4. This finding is consistent with the notion that single platelets are the smallest particles expected. The computed particle size distributions agree well qualitatively and in most cases agree quantitatively with experimental observations. The model correctly predicts the shifting of the curves and the area beneath the curves. The agreement is best in the large size range, since the objective function chosen gives weight to the deviations in proportion to particle volumes.

In conclusion, aggregation agents, temperature, shear history, and shear rate are among the factors which influence platelet aggregation and disaggregation. This study has provided information on how shear forces influence platelet aggregation and disaggregation. The PBE model, despite its simplifications, provides another way for studying platelet kinetics in the presence of chemical and physical stimuli. The reversible model developed here can be solved numerically, and used to monitor platelet aggregation and disaggregation. The model seems to have the potential to become a valuable tool in characterization of the state of platelet activity. Hence, it may be useful in efforts to understand thrombotic and hemostatic processes, and to develop agents for therapy and prophylaxis.

GLOSSARY

Nomenclature

$g(v)$ breakage frequency, s^{-1}
k_1 breakage rate constant in Eq. 4, sec^{-1}
$\tilde{k}$ erosion rate constant in caption of Fig. 3, dimensionless
m order of breakage rate in Eq. 4, dimensionless
v, w particle volume, μm^3
x dimensionless particle size, v/v_o
x_{ss} maximum stable particle size in Eq. 5 (no breakage for $x \leq x_{ss}$), dimensionless

Greek symbols

γ average number of fragments formed by breakage, dimensionless
ϕ void fraction related to collision diameter, dimensionless

This work was supported by the National Institutes of Health under grants 5P50NS23327 and 5R3718584.

REFERENCES

1. Huang, P. Y., and J. D. Hellums. 1993. Aggregation and disaggregation kinetics of human blood platelets: Part I. Development and validation of A population balance method. *Biophys. J.* 65:334–343.
2. Huang, P. Y., and J. D. Hellums. 1993. Aggregation and disaggregation kinetics of human blood platelets. Part II. Shear-induced platelet aggregation. *Biophys. J.* 65:344–353.
3. Austin, L. G. 1971. A review: introduction to the mathematical description of grinding as a rate process. *Powder Technol.* 5:1–17.
4. Andrea-Villegas R., and R. D. Letterman. 1976. Optimizing flocculator power input. *J. Envi. Eng., Proc. Am. Soc. Civ. Engrs.* 102:251–263.
5. Argaman, Y., and W. J. Kaufman. 1970. Turbulence and flocculation. *J. San. Eng. Div., Proc. Am. Soc. Civ. Engrs.* 96(SA2):223–241.
6. Parker, D. S., and W. J. Kaufman. 1972. Floc breakup in turbulent flocculation processes. *J. San. Eng. Div., Proc. Am. Soc. Civ. Engrs.* 98(SA1):79–99.
7. Kao, S. V., and S. G. Mason. 1975. Dispersion of particles by shear. *Nature.* 253:619–621.
8. Quigley, J. E. 1977. Strength properties of liquid borne flocculated matter. M.S. thesis. University of Delaware, Newark. p. 100.
9. Glasgow, L. A., and R. H. Luecke. 1977. Mechanism of deaggregation for clay-polymer flocs in turbulent systems. *Ind. Eng. Chem. Fundam.* 19:148–156.

10. Thomas, D. G. 1964. Turbulent disruption of flocs in small particle size suspensions. *A. I. Ch. E. J.* 10:517–521.
11. Valentas, K. J., O. Bilous, and N. R. Amundson. 1966. Analysis of breakage in dispersed phase systems. *Ind. Eng. Chem. Fund.* 5:271–279.
12. Pandya, J. D., and L. A. Spielman. 1982. Floc breakage in agitated suspension: theory and data processing strategy. *J. Colloid. Int. Sci.* 90:517–531.
13. Pandya, J. D., and L. A. Spielman. 1983. Floc breakage in agitated suspensions: effect of agitation rate. *Chem. Eng. Sci.* 38:1983–1992.
14. Akers, R. J., A. G. Rushton, and J. I. T. Stenhouse. 1987. Floc breakage: the dynamic response of the particle size distribution in a flocculated suspension to a step change in turbulent energy dissipation. *Chem. Eng. Sci.* 42:787–798.
15. Nichols, A. R., and H. B. Bosmann. 1979. Platelet aggregation: newly quantified using nonempirical parameters. *Thromb. Haemost.* 42:679–693.
16. Nguyen, P. D., and E. A. O'Rear. 1990. Temporal aggregate size distribution from simulation of platelet aggregation and disaggregation. *Ann. Biomed. Eng.* 18:1–18.
17. Huang, P. Y. 1991. The kinetics of human platelet aggregation and disaggregation in controlled shear field. Ph.D. thesis. Rice University, Houston, TX. p. 23.